Int. J. Heat Mass Transfer. Vol. 28, No. 4, pp. 823–836, 1985
Printed in Great Britain

0017–9310/85 $3.00 + 0.00
Pergamon Press Ltd.

Numerical and experimental studies on a two-dimensional model of an offset-strip-fin type compact heat exchanger used at low Reynolds number

K. SUZUKI, E. HIRAI and T. MIYAKE
Department of Mechanical Engineering, Kyoto University, Kyoto 606, Japan

and

T. SATO
Department of Mechanical Engineering, Setsunan University, Neyagawa, Osaka, Japan

(*Received* 27 *April* 1984 *and in final form* 18 *August* 1984)

Abstract—Numerical and experimental studies have been made on the flow and heat transfer characteristics of a two-dimensional system with a staggered array of vertical flat plates used in the free–forced mixed convection regime at low Reynolds number. The numerical schemes presently used are validated through the comparisons between their numerical results and the corresponding experimental data which were also obtained in the present study. Through these comparisons, the effects of fin thickness and free-stream turbulence are discussed. Comparisons are also made between the present two-dimensional computation and the experimental data for a practical offset-strip-fin type compact heat exchanger and comments on the effects of three-dimensionality are added. Discussions on the effects of some geometrical parameters of heat exchanger on its performance are finally presented based on the present numerical works.

1. INTRODUCTION

IN CONNECTION with the practical demand for the development of high performance heat exchangers, experimental studies have been made on the flow and heat transfer performance of offset-strip-fin type compact heat exchanger by London and Shah [1] and Mochizuki and Yagi [2]. Related basic studies have also been carried out experimentally and theoretically for the two-dimensional heat transfer system with a staggered array of flat plates by Sparrow *et al.* [3], Sparrow and Prakash [4], Cur and Sparrow [5] and Patankar and Prakash [6]. The present work is similar to these studies but differs from them in several points.

All the above studies are concerned with pure forced or free convection flow regimes. In ref. [7], however, a numerical study was made on the performance of a vertically mounted two-dimensional heat transfer system with a staggered array of flat plates of zero thickness, and it was demonstrated that the free–forced mixed convection flow regime can easily be established at low Reynolds number ($Re < 1000$). The free–forced mixed convection was found to be effective in reducing the magnitude of pressure loss inside the heat transfer system as well as aiding the heat transfer. The reduction of pressure loss is especially favourable for the heat exchanger which is to be used to recover thermal energy from waste gas. The reduction of the power required for feeding the waste gas is one of the important factors affecting the net amount of energy to be recovered and mitigating the necessary amount of investment. The present study is an extension of the previous work reported in [7] and deals with the free–forced mixed convection flow regime. In the final part of the present article, the effects of some geometrical parameters unexamined in [7] will be discussed.

The present study is composed of numerical work and experimental work. Except for the work done by Patankar and Prakash [6], no comparison has been undertaken between the theoretical and experimental results. Patankar and Prakash compared their numerical results for a two-dimensional heat transfer system with the experiments done by London and Shah for the practical offset-strip-fin type heat exchanger. A rather large discrepancy was found between the two results, but they did not give detailed discussions for the reasons of this. Such a discussion requires firstly quantitative validation of the used numerical computation scheme and for this purpose, some experimental data for the two-dimensional system are required. Thus, an experimental study was carried out in addition to the numerical study and its results will be discussed in the main part of the present paper in comparison with the numerical counterparts.

First, two problems which are important from the practical viewpoint will be discussed. They are the effects of the fin thickness and the free-stream turbulence. In the discussions of these effects, some experimental data will also be compared with their numerical counterparts. Based on these preparations, further comparison will be made between the present numerical computation for a two-dimensional system and the experiments for the practical compact heat exchanger reported in [1]. This comparison provides a

NOMENCLATURE

A total heat transfer area
A_f fin surface area
B fin spanwise length
C_1, C_2, C_μ constants
C_p specific heat at constant pressure
$\bar{C}_p$ local pressure loss coefficient
$\bar{C}_p^*$ total pressure loss coefficient
f apparent friction coefficient
g gravitational acceleration
Gr Grashof number
Gr^* modified Grashof number
H total depth of heat transfer system
h local heat transfer coefficient
j Colburn's j-factor
k turbulence kinetic energy
L fin offset length
L_ε dissipation length scale of turbulence, $2k^{3/2}/\varepsilon$
M rod pitch of turbulence grid
N total number of rows of flat plates or fins
Nu local Nusselt number
Nu^* local Nusselt number given by equation (2)
$\overline{Nu}$ mean Nusselt number
P static pressure
ΔP pressure correction
Pr Prandtl number
q_w wall heat flux
Re Reynolds number
Re^* Reynolds number based on the hydraulic diameter and on the averaged gas velocity inside the heat transfer system
S half of the distance of the centre lines between two neighbouring plates
St Stanton number
T temperature
Tu turbulence level
t time
U velocity component in x-direction
V velocity component in y-direction
x streamwise coordinate
x_i Cartesian coordinate ($i = 1, 2, 3$)
y spanwise coordinate.

Greek symbols
β cubic expansion coefficient
ε isotropic part of dissipation rate of turbulence kinetic energy
η recovery factor of thermal energy
λ thermal conductivity
μ_t turbulent eddy viscosity
ν kinematic viscosity
ξ area ratio representing the density of heat transfer surface
ρ density
σ_{ht} turbulent Prandtl number
σ_{kt} counterpart of σ_{ht} for k
$\sigma_{\varepsilon t}$ counterpart of σ_{ht} for ε
ψ stream function
ω vorticity.

Subscripts
0 approaching flow
$\bar{}$ mean value
m bulk mean condition
w fin surface.

basis for further analysis regarding the effect of three-dimensionality of the practical heat exchanger.

The present numerical computation differs from the works [3] and [4] in that it solves the elliptic type of differential equations governing the momentum and enthalpy of the fluid. The present computation is executed for the whole heat transfer system with multiple rows of fins. In this respect, the present computation is quite different also from the work by Patankar and Prakash [6], who did the computation only for a single module in the fully developed region of flow and thermal fields to be established for the module deep in the system.

2. EXPERIMENTAL APPARATUS AND PROCEDURE

A schematic view of the experimental apparatus is shown in Fig. 1. A vertical heat transfer system having three rows of flat plates, arranged in a staggered pattern was located in upward air flow in a low speed wind tunnel. Each flat plate is an acrylic plate sandwiched

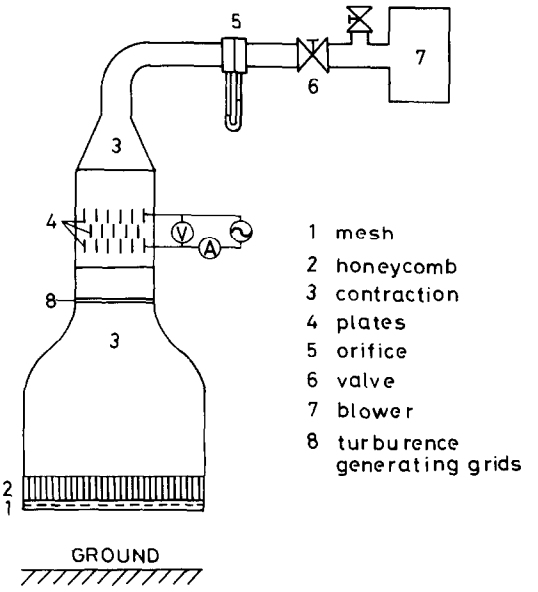

FIG. 1. Schematic view of the experimental set-up.

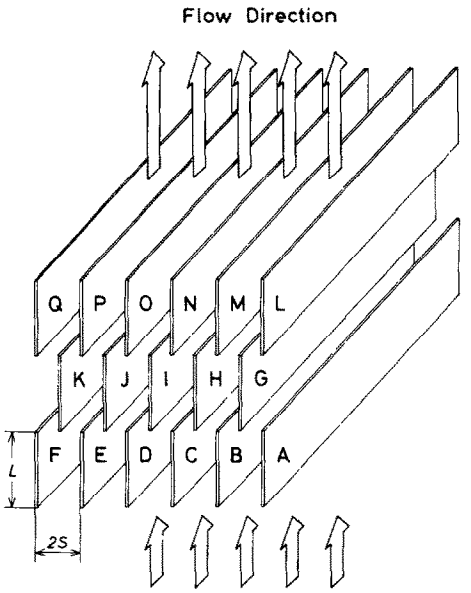

FIG. 2. Two-dimensional array of staggered flat plates.

between thin metal sheets of 30 μm thickness and has the streamwise width $L = 50$ mm and the spanwise length $B = 400$ mm. The former length is called sometimes fin offset length. Experiments were carried out for the two systems of different flat plate thickness, i.e. 1 mm and 4 mm. The pitch of the flat plates, the distance between the centre lines of two neighbouring plates, was kept constant at $2S = 30$ mm for these two systems. A sketch of the staggered array of plates is given in Fig. 2.

The metal sheets functioning as the heat transfer surface were heated by passing an alternating electric current through them. Each sheet was heated at uniform heat flux condition within an accuracy of about 3%. The five flat plates named C, D, I, N and O in Fig. 2 were used as the main test plates. Seven thermocouples were attached to the back surface of each sheet glued to these five flat plates along their streamwise centre lines and were used to measure the streamwise distribution of heat transfer surface temperature. A number of other thermocouples were attached to the same plates in a similar manner but at positions off their centre lines and also to other flat plates. These were used to check the uniformity of the thermal field in a plane normal to the flow direction. As a whole, the outputs from these thermocouples show that the thermal field can be taken as two-dimensional, but irregular non-uniformity was still found among the outputs of the thermocouples located at the same streamwise positions. This can lead to an error in the local Nusselt number of about 10% at worst. Thus, the local Nusselt number was calculated for each streamwise location with the average of the outputs from the set of thermocouples provided at the same streamwise position but at different spanwise positions or on the different plates.

The Reynolds number, Re, the local Nusselt number, Nu^*, and the modified Grashof number, Gr^*, to be used in the presentation of the experimental results are defined as follows:

$$Re = \frac{4SU_0}{\nu_0} \tag{1}$$

$$Nu^* = \frac{4S|q_w|}{\lambda_0|T_w - T_0|} \tag{2}$$

$$Gr^* = \frac{(4S)^4 g\beta_0|q_w|}{\lambda_0 \nu_0^2} \tag{3}$$

where U_0 is the volume flux of air calculated on the basis of the hollow cross sectional area inside heat exchanger; ν_0, λ_0 and β_0 are respectively the kinematic viscosity, the thermal conductivity and the cubic expansion coefficient of air evaluated at the inlet temperature T_0; q_w is the wall heat flux at the plate surface and g is the gravitational acceleration. The representative length $4S$ introduced in the above definitions corresponds to the hydraulic diameter of an ideal two-dimensional channel between the two parallel plates separated by the pitch $2S$.

The volume flow rate of air was measured with an orifice, 5 in Fig. 1. The density of air at the location of orifice is smaller than the inlet air density and was determined by taking account of the total heating power input. To study the influence of free-stream turbulence on the heat transfer, square-mesh turbulence grids made of 5 × 5 mm square rods were inserted 500 mm below (i.e. upstream) of the heating system. Three different turbulence grids having mesh pitches 12 mm, 18 mm and 24 mm were tested. These pitches were chosen considering that the possible flow disturbing sources in practical situations are likely to have the dimension similar to the fin pitch of the heat exchanger.

Almost all experiments were carried out at the Reynolds number below 1000. However, in this range of Reynolds number, the fluctuating signal from the hot-wire anemometer was so weak that its signal-to-noise ratio could not be brought high enough to confirm the effectiveness of the used grids in generating turbulence. Thus, an additional experiment was conducted at $Re = 3700$ for the measurement of the free-stream turbulence effect on heat transfer.

3. NUMERICAL COMPUTATION SCHEME

In the present study, two different numerical schemes have been used. One of them is a new version of the one used in the previous study [7], which solves the governing equations of elliptic type differential equations for the stream function ψ and the vorticity ω, the so called ψ–ω method. The new version can treat a transfer system composed of the flat plates with finite thickness. The second numerical scheme is a modified version of the one used for the computation of turbulent heat transfer in recirculating flows [8, 9], which solves the axial and normal velocity components U and V

together with the pressure correction ΔP, the so called U–V–P method. The latter scheme was prefered in the calculation of turbulence effects because it is easier to incorporate the turbulence model. The turbulence model used in the old version was replaced by a low Reynolds-number turbulence model, to be described later, in order to deal with the turbulent flow at low Reynolds number. The first scheme is based on the method described by Gosman *et al.* [10] and the second one origined from the 2/E/FIX code developed by Pun and Spalding [11]. The details of the basic part of each method can be found in refs. [7–11]. Therefore, a brief description outlining the difference between the present schemes and their original counterparts will be given below.

Figure 3 shows the computation domain adopted in the present study. In this domain, a maximum of 339 $\times$ 31 grid points were allocated non-uniformly such that finer grid spacing is provided near the leading and trailing edges of each plate in x-direction and near the plate in y-direction. The non-uniformity of pressure field around the leading edges of flat plates in the first row can affect the flow upstream [12]. To assume uniform inlet flow velocity and enthalpy, the upstream boundary was located at a position where the flow is free from the effects of such a non-uniform pressure field. The downstream boundary was located at a position of three times the streamwise width of the flat plate downstream from the trailing edges of the plates in the last row. The downstream boundary condition was set by a method similar to that used in the references [13, 14], which assumes that the flow there is governed by the parabolic differential equation. Alternating

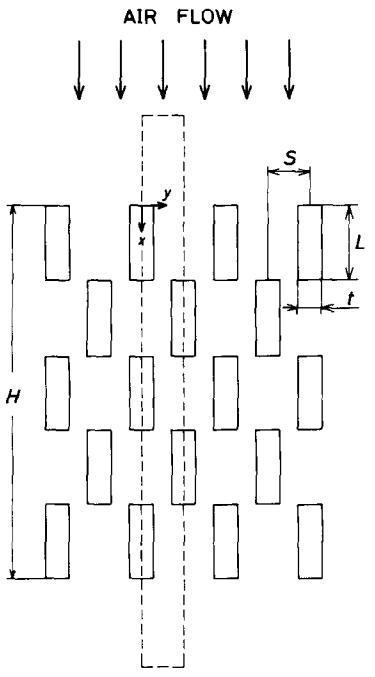

FIG. 3. Computation domain.

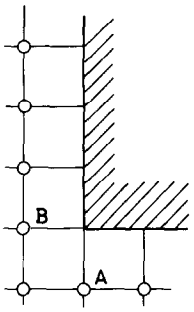

FIG. 4. Illustration of the grid points around corner.

protrusion of solid body into the flow space occurs periodically when the finite thickness of the plate is taken into account. A wall boundary condition similar to that used in the previous study for the case of zero plate thickness was applied to both of the plate surfaces parallel and normal to the flow direction. One difference is the boundary condition for the vorticity at the corner of the flat plate. In the previous study, a linear distribution of vorticity was assumed near the solid surface. At the corner, there are two neighbouring grid points inside the flow domain as shown in Fig. 4; one is located on the streamwise grid line passing the corner (point A) and another is located on the grid line normal to the flow direction and passing the same corner (point B). Assuming the linear distribution of ω, two values of vorticity ω_A and ω_B can be assigned for each corner. ω_A is the value of vorticity related linearly to the vorticity at the point A and ω_B is the one related linearly to the vorticity at the point B. Both of these two assigned values of vorticity were used for any corner in the following manner. ω_A was used as the boundary condition for the vorticity conservation in the cell surrounding the grid point A, while ω_B was used in same way for the cell surrounding the grid point B. This method was compared with other methods to treat the vorticity at the corner described by Roache [15]. The calculated results with all such methods were only slightly different from each other but the presently adopted method was found to be stable and to lead to better convergence. Incidentally, Patankar proposed a method of treating a solid body protruding into the flow passage [16]. He took the solid protrusion as a part of the fluid having very large viscosity and assigned the harmonic mean of the solid and fluid thermal conductivities to the interface thermal conductivity. This method was also examined in the present study by incorporating it into the U–V–P scheme. However, this method was found to cause a numerical instability in iteration process when the plate thickness becomes large. This may have resulted from an inappropriate variation of pressure correction during the iteration. Although the flow induced in the calculation in the solid part is certainly very weak, it still results in an incomplete overall mass conservation of real fluid. This is because there is no specification of velocity or stream

function at the solid–fluid interface. Thus, an error is caused for the pressure correction which is determined so as to satisfy the continuity equation. Additionally, this method is not so useful for the heating condition at uniform wall heat flux. Therefore, this method was finally abandoned in the present computation.

In the computation of the free-stream turbulence effect, the following set of the equations for the turbulence kinetic energy k and its dissipation rate ε is employed.

$$\frac{Dk}{Dt} = \frac{1}{\rho}\frac{\partial}{\partial x_j}\left(\frac{\mu_t}{\sigma_{kt}}\frac{\partial k}{\partial x_j}\right) + \frac{\mu_t}{\rho}\left(\frac{\partial U_i}{\partial x_j} + \frac{\partial U_j}{\partial x_i}\right)\frac{\partial U_i}{\partial x_j} - \varepsilon - 2\nu\frac{\partial k^{1/2}}{\partial x_j}\frac{\partial k^{1/2}}{\partial x_j} \quad (4)$$

$$\frac{D\varepsilon}{Dt} = \frac{1}{\rho}\frac{\partial}{\partial x_j}\left(\frac{\mu_t}{\sigma_{\varepsilon t}}\frac{\partial \varepsilon}{\partial x_j}\right) + \frac{C_1\mu_t}{\rho}\frac{\varepsilon}{k}\left(\frac{\partial U_i}{\partial x_j} + \frac{\partial U_j}{\partial x_i}\right)\frac{\partial U_i}{\partial x_j} - C_2\left[1 - 0.3\exp\left(-\frac{k^4}{\nu^2\varepsilon^2}\right)\right]\frac{\varepsilon^2}{k} \quad (5)$$

where the tensor notation has been used, D/Dt is the substantial derivative, U_i the mean velocity along the coordinate x_i, σ_{kt} and $\sigma_{\varepsilon t}$ the counterparts of the turbulent Prandtl number respectively for k and ε, ν the kinematic viscosity of the fluid, and μ_t the turbulent eddy viscosity defined with the values k and ε in the following manner:

$$\mu_t = C_\mu \exp\left[-\frac{125}{50 + \frac{k^2}{\nu\varepsilon}}\right]\frac{\rho k^2}{\varepsilon}. \quad (6)$$

The chosen values of the constants C_1, C_2 and C_μ in the above equations are the same as those found in ref. [17]. The above set of equations (4) and (5) is almost the same as the model proposed by Launder and Spalding [17] except for one point. One viscous term has been omitted from the equivalent of equation (5), the governing equation for the isotropic part of the dissipation rate of turbulent kinetic energy following the expression by Jones and Launder [18]. It is governed by the energy transfer rate in the wave number space in the direction from large energy containing eddies to smaller ones. This rate should be free from the viscous effects. This is the major reason for dropping the term. Additionally, the dropped term includes the second derivatives of mean velocities. From the numerical view point, the dropped term is likely to cause numerical instability. Plumb and Kennedy [19] succeeded in predicting turbulent free convection on a vertical flat plate but, in the present study, the thermal effects on the turbulence considered by them has been ignored. This is because it is uncertain if their model for high Rayleigh number flow can work for the turbulence at low Reynolds number presently concerned.

The boundary conditions for k and ε at the flat plate surface were given by $k = \varepsilon = 0$. Zero values were also assigned to the wall values of U and V. The normal gradient of ΔP at the wall was set equal to zero [11]. In the computation of a case when the flat plate is heated or cooled at uniform wall temperature, the wall enthalpy was given and the wall heat flux was computed from the fluid temperature gradient at the interface. In another case when the flat plate is heated or cooled at uniform heat flux, the wall heat flux was accounted as the source term for the enthalpy balance in the grid cell adjoining the flat plate and the surface temperature was computed through the iteration. The boundary conditions for the above variables at other boundary positions were given similarly to those used in the first scheme.

Since the present experiments were performed for upward flow heated by the heat transfer system, the numerical computations to be compared with such experimental results were also done for the upward flow. In the present computation, the Boussinesq approximation is not used because it does not have wide validity [23]. Therefore, as shown in ref. [7], upward heated flow is not equivalent to downward cooled flow. In the computation whose results will be discussed in the last part of the present paper, attention was paid to the downward flow from which thermal energy is extracted by the heat transfer system. This is an interesting situation from the practical view point as has been mentioned already. In the computations, the temperature of the flat plates mounted in staggered array was assumed to be kept at uniform temperature. The temperature level of the flat plate will be presented with the Grashof number Gr defined below. In the discussions of the results of such computations, the averaged Nusselt number $\overline{Nu}$ and the pressure loss coefficient $\overline{C_p^*}$ will be introduced.

$$Gr = \frac{(4S)^3 g\beta_0|T_w - T_0|}{\nu_0^2} \quad (7)$$

$$\overline{Nu} = \frac{1}{H}\sum_{i=1}^{N}\int_{(i-1)L}^{iL} Nu\, dx \quad (8)$$

$$\overline{C_p^*} = \frac{1}{2S}\int_0^{2S}\frac{P_{x=H} - P_0 - \rho_0 gH}{\rho_0 U_0^2}\, dy \quad (9)$$

where

$$Nu = \frac{4S|q_w|}{\lambda_m|T_w - T_m|}.$$

In the above equations, H is the total depth of the heat transfer system and N is the row number of the flat plates or fins, so that $H = NL$. Integration over the space $2S$ was introduced to account for the fact that the pressure distributes non-uniformly across the flow passage [7]. Since the static head $\rho_0 gH$ has been subtracted in equation (9), $\overline{C_p^*}$ approximately expresses the level of the pressure loss caused by an introduction of the heat transfer system into the flow line of waste gas. Its positive value yields a pressure gain as a result of the superposed free convection which drives the fluid naturally.

4. COMPARISONS BETWEEN NUMERICAL COMPUTATION AND EXPERIMENT

It may be worthwhile to compare first the results of the two numerical schemes used in the present study with each other. Figure 5 shows an example of such a comparison. The two computed distributions of local Nusselt number were obtained for a common case; the upward flow at $Re = 500$, heated by the three-row staggered array of the vertical flat plates with zero thickness. The flat plate surface was assumed to be maintained at a uniform heat flux corresponding to $Gr^*/Re^2 = 80$. The two results agree very well with each other. This proves that the difference in the computation scheme is not important in discussing the computed results.

In the previous study, the free–forced mixed convection was demonstrated to be effective in reducing the pressure loss occurring inside the heat transfer system as well as in aiding the heat transfer [7]. However, any validation of the numerical scheme was not given. Figure 6 shows the comparison between the experimental data of local Nusselt number presently obtained for upward heated flow and its corresponding numerical one. Since the actual thickness of the plate in the experiment was thin such that $t/2S = 0.033$, zero thickness of the plate was assumed in the computation. The good agreement between the experiment and the numerical computation validates the numerical scheme used in the previous and present studies, at least, for the case of a thin flat plate. Considering that the relationship $Gr^* = Gr\ Nu^*$ holds and that the average Nusselt number for this case is approximately 25, the value of Gr^*/Re^2 chosen in this case is approximately equivalent to $Gr/Re^2 \cong 6$. Comparing this with the results of the previous study [7], the flow attained in this experiment is believed to be in the free–forced mixed convection regime.

Figure 7 shows the distribution of the local Nusselt number presently obtained experimentally for the heat transfer system having thicker plates. Its numerical counterparts are also shown for the two cases of the

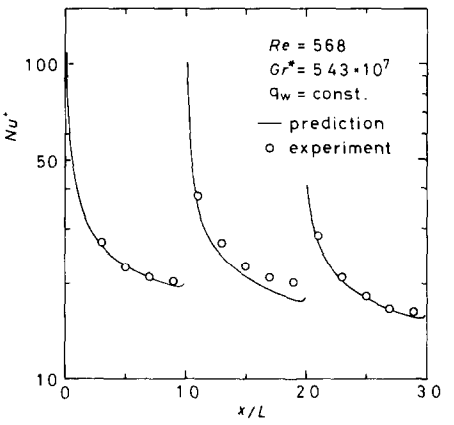

FIG. 6. Comparison for the heat transfer system with thinner flat plates.

plate thickness $t/S = 0.0$ and $t/S = 0.267$. Although the experiment shows higher values of Nu compared to the numerical results, this degree of discrepancy may be tolerable and does not significantly detract from the following discussion of the present numerical results, even for the heat transfer system with finite thickness of the plates. Comparing the experimental results plotted in Fig. 7 with those in Fig. 6 for the system having thinner plates, it may be concluded that the effects of flat plate thickness is rather small, at least, within the range of the thickness tested in the present experiment. Numerical results also show that the difference in plate thickness does not cause significant change in heat transfer results. In connection with this, another comparison is shown in Fig. 8 of the numerical results of local Nusselt number for the three different cases of plate thickness. The chosen value of L/S is smaller in this figure than in Fig. 7. There are noticeable differences among the three results around the trailing edge of each plate but the difference in the averaged Nusselt number caused by the change in t/S is concluded to be rather small within its range to be encountered in practices. Incidentally, flow separation leading to heat transfer deterioration was initially

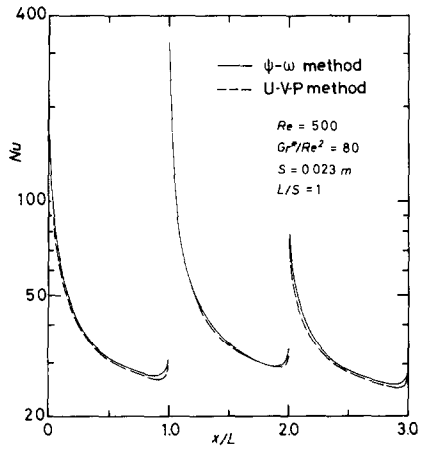

FIG. 5. Comparison of two numerical schemes.

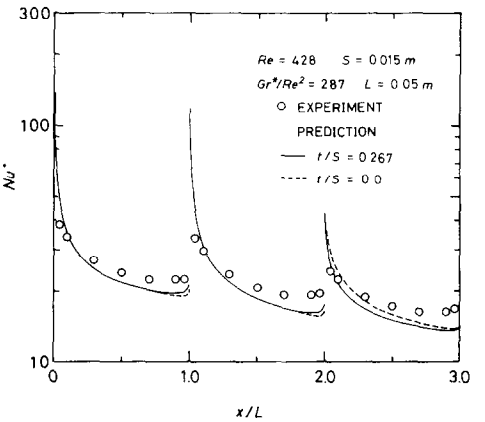

FIG. 7. Comparison for the heat transfer system with thicker flat plates.

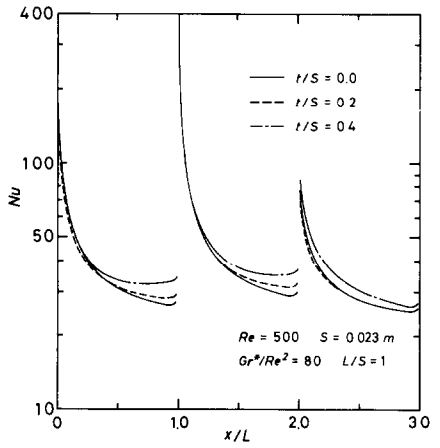

FIG. 8. Effects of flat plate thickness on local Nusselt number.

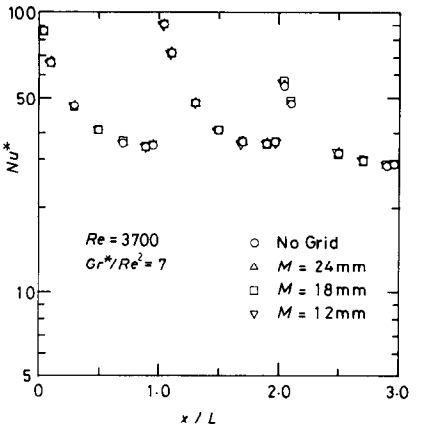

FIG. 10. Effects of free-stream turbulence at elevated Reynolds number.

suspected to occur at a position close to the leading edge of each plate, more likely so when the plate is thicker. However, it is felt reasonable to conclude that such heat transfer deterioration is not significant at the Reynolds numbers presently studied. No symptom of such flow separation was found in the calculated velocity field, even in the case of the thickest plate. Experimental heat transfer data did not show any significant difference between the two cases of different plate thickness. At rather low Reynolds number presently considered, non-uniform pressure field formed around the leading edge of the plate [12] would have accelerated the flow just after the leading edge and have suppressed the flow separation there. Additional discussions on the effects of the plate thickness will be given later.

Figure 9 shows the experimental results of the local Nusselt number for four cases; one for the case using no turbulence generating grid and others for the three cases using turbulence grids of different rod pitch. It is seen that the insertion of a turbulence grid affects the heat transfer characteristics very little. The chosen value of Reynolds number in this comparison is not high enough, as mentioned before, to confirm that the turbulence grids effectively produce free-stream turbulence. Thus, another experiment was performed at $Re = 3700$ and the obtained results are shown in Fig. 10. To protect the heat transfer surface from thermal damage, the value of Gr^*/Re^2 was set equal to 7. This value is sufficiently low that the flow observed in this additional experiment was of the pure forced convection regime. At this Reynolds number, the turbulence intensity Tu observed at the inlet to the array was 1.3% when no turbulence grid was used but it was experimentally confirmed to be 4.8, 4.4 and 4.1% respectively in the cases with the turbulence grids of rod pitch $M = 24, 18$ and 12 mm. Figure 8 indicates that the free-stream turbulence affects the value of Nu very little even at this higher Reynolds number.

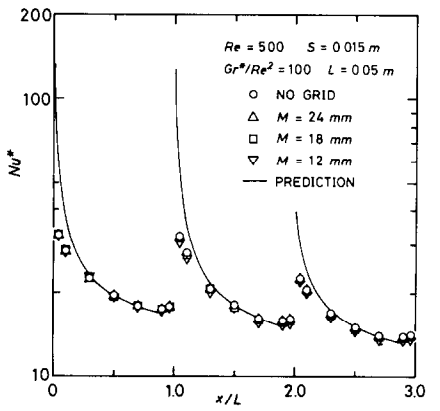

FIG. 9. Effects of insertion of turbulence grid on local Nusselt number.

In Fig. 9 a numerically obtained result is also plotted. In this computation, the level of the streamwise velocity fluctuation normalized by the streamwise mean velocity, Tu, was assumed to be 1%. This value of Tu corresponds to the value obtained experimentally with a hot-wire anemometer. The length scale of turbulence L_ε used for the determination of ε [20] for the inlet flow was assumed to be 2.7 cm. This value of L_ε does not contradict with the assumption that the length scale of practically possible flow disturbing source, and therefore of turbulence, is closed to the fin pitch $2S$. The numerical results agree fairly well with the experimental results. Further examination was made numerically for the effects of the turbulence intensity and length scale of the free-stream turbulence. Such results are tabulated in Table 1. The symbol * in the table means that good converged result could not be obtained. The tabulated averaged Nusselt number differs very little from one to another and this indicates that the heat transfer characteristics are affected little by the free-stream turbulence within the examined ranges of its intensity and length scale.

In Fig. 11, a comparison is given between the present two-dimensional numerical computation and the experimental results by London and Shah for practical

Table 1. Comparison of mean Nusselt number $\overline{Nu}$

L_ε (cm)	Tu 2%	4%	6%
2.70	42.08	41.98	—
1.80	42.11	41.94	—
0.90	42.00	41.94	41.88

offset-strip-fin compact heat exchanger used in pure forced convection flow regime. Since no information is available for the free-stream turbulence in their report, the equations for k and ε were not solved in this particular computation. However, this is not crucial because its effect has just been shown to be small. Schematic illustration of the practical heat exchanger treated by London and Shah is given in Fig. 12. In the computation, $B/4S$ was assumed infintely large but the fin efficiency was taken to be unity. Preliminary study based on heat conduction theory and an estimated average Nusselt number has shown that the fin efficiency is very close to unity. In the reported experimental results, the friction factor f and the heat transfer factor j are defined as the averaged values over the total heat transfer surface area A. However, the present computation gives their values only for the fin surface area A_f. Therefore, the computed values of f and j must be converted into their equivalents corresponding to the presented form of experimental results. This was carried out simply by multiplying each by the ratio A_f/A. This is not likely to cause significant error because the fraction $(1-A_f/A)$ is smaller than another fraction A_f/A and the velocity and thermal boundary layers are much thicker on the area $(A-A_f)$ than on the fin surface area A_f. Additionally, all the results are presented against the Reynolds number Re^*, which is defined with the hydraulic diameter of the practical heat exchanger as the representative length. The number of fin rows was reported in the ref. [1] to be in the range $12 \leqslant N \leqslant 52$. Since the effect of the value of N on the heat transfer performance will be shown later to be small when $N \geqslant 13$, N was set equal to 15 in this computation. Furthermore, in this computation, the variation of fluid properties with gas temperature was not considered and they were evaluated at the room temperature. This is because the correct level of gas temperature is not available in [1].

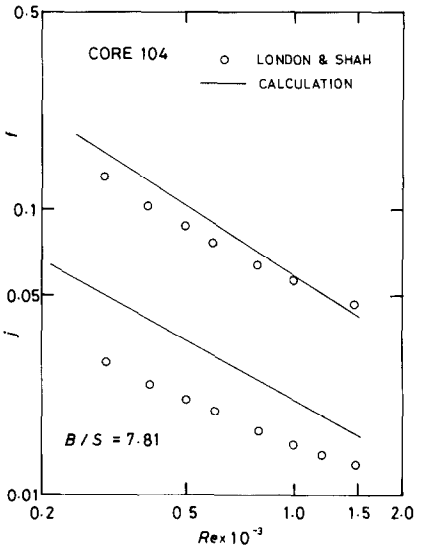

FIG. 11. Comparison with the experiments by London and Shah.

The present computation agrees well, qualitatively, with the experiments of London and Shah and seems to be better than the computation given by Patanker and Prakash for a single module located deep in the heat exchanger [6]. Their computation shows steeper dependence of f and j on Reynolds number. In Fig. 11, better agreement with experiment is found for f than for j. Another similar comparison is given in Fig. 13, in which the present numerical results are compared again with the experiments by London and Shah but for the offset-strip-fin compact heat exchanger of another geometry. In this comparison, better agreement is found for the heat transfer characteristics and for the

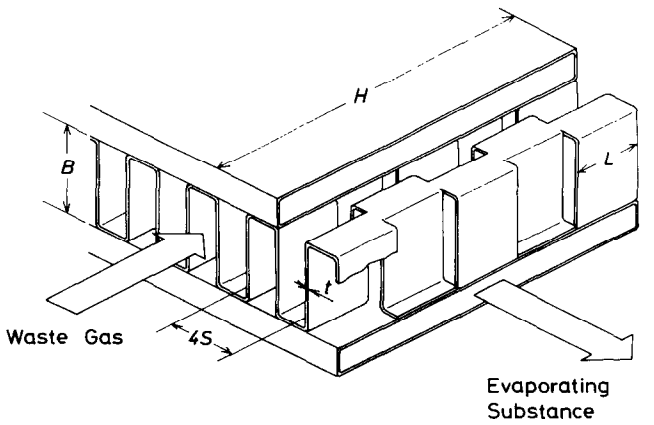

FIG. 12. Schematic view of offset-strip-fin type compact heat exchanger.

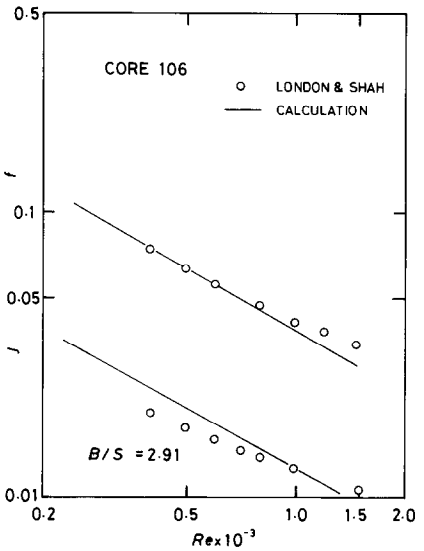

FIG. 13. Comparison with the experiments by London and Shah [1].

apparent friction factor compared to the previous figure, although the span ratio $B/4S$ of this case is smaller. The reason for this inconsistency between Figs. 11 and 13 may not be attributed only to the inadequacy of the present numerical computation. Yang [21] suggested that the heat transfer is enhanced by the unsteady flow incurred in the wake of each fin at the Reynolds number above about 100. Since, in Fig. 11, the present computation shows higher value of j than its experimental value, this cannot be confirmed directly. He also suggested that the dependency of f and j on Reynolds number becomes milder in the second laminar flow regime where the flow becomes unsteady. Mochizuki and Yagi [22] performed flow vizualization experiments for the arrays of staggered flat plates and found that the flow becomes unsteady at the Reynolds number Re_t, based on the plate thickness, above 50. Considering that the heat exchanger used in the experiments of Fig. 11 has the fin thickness to hydraulic diameter ratio 0.043, the critical value of Re^* for the onset of unsteady flow is estimated around 1100. Therefore, the onset of unsteady flow does not contribute to the inconsistency pointed out above, at least in the range of Re^* below 800 where the computation of f shows good qualitative agreement with the experimental results. The practical heat exchanger might have geometrical inaccuracy. This may affect both of its heat and flow characteristics. In addition to this, contact heat transfer resistance between the fins and the base body cannot be ignored for practical heat exchanger. These have some non-reproducible character and may partially contribute to the inconsistency in discussion. Three-dimensionality of the practical heat exchanger is certainly one of the causes of the discrepancy between the presently computed value and the experimental counterpart. Thus, it may be interesting to carry out the three-dimensional computation in future. However, the good qualitative agreement between the present computation and the experiment found in low Reynolds number range suggests that the present two-dimensional computation is still available to learn how geometric parameters can affect the performance of heat exchanger. From this view point, more detailed discussions will be given below on the effects of some geometric parameters for the two-dimensional heat transfer system with staggered array of flat plates used in the free–forced mixed convection regime.

5. EFFECTS OF GEOMETRIC PARAMETERS

First, the effects of fin or plate thickness will be addressed, which has partially been discussed above. For the three cases whose heat transfer results have been presented in Fig. 8, the simultaneously computed distribution of local pressure loss coefficient $\overline{C_p}$ are plotted in Fig. 14. The definition of $\overline{C_p}$ is as follows:

$$\overline{C_p} = \frac{1}{2S}\int_0^{2S} \frac{P - P_0 - \rho_0 g x}{\rho_0 U_0^2}\,dy. \qquad (10)$$

As is found most remarkably in the case of thickest plates, pressure loss occurs at the positions corresponding to the leading and trailing edges of each plate. This is a main cause of large total pressure loss for the system with thicker plates. For the reasons mentioned previously, larger pressure loss is undesirable for a heat exchanger which is to be used for the recovery of thermal energy from waste gas. As also pointed out previously, an increase of local Nusselt number occurs around the trailing edge, especially for the first and second plates, when t/S is increased. However, it is also perceived that the average Nusselt number does not vary so remarkably with an increase of t/S. Therefore, there is no good reason to prefer thicker fins.

The fin thickness to hydraulic diameter ratio 0.043 of Fig. 11 corresponds to the value of $t/2S$ below 0.2. Figures 8 and 14 indicate that the heat transfer and flow characteristics of the heat transfer system having the value of $t/2S$ below 0.2 can be approximated by the ones computed for the case of $t/2S = 0.0$. For this reason, the following discussions about the effects of other

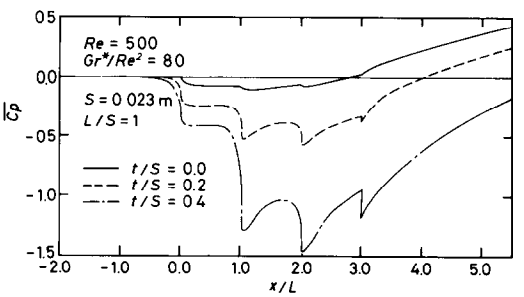

FIG. 14. Calculated local pressure loss coefficient.

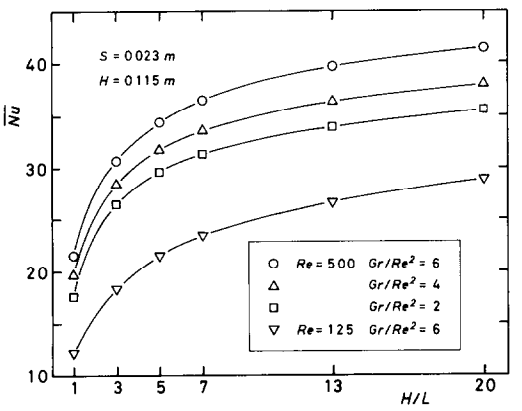

FIG. 15. Change of average Nusselt number with the offset length L.

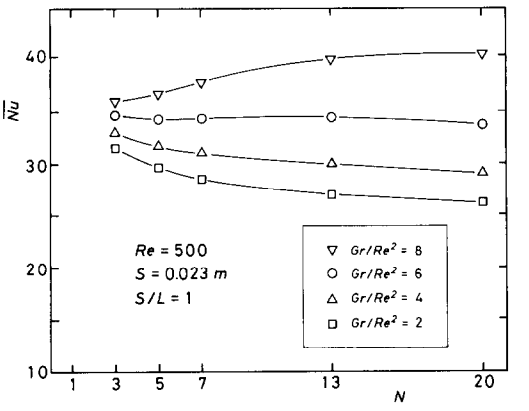

FIG. 17. Change of $\overline{Nu}$ with the total depth H.

geometrical parameters will be given based on the computations for the heat transfer system having staggered array of flat plates with zero thickness. In these computations, the Reynolds number and the value of Gr/Re^2 were also changed.

Incidentally, the value of Gr/Re^2 is about 3 in the computations plotted in Fig. 14. This is a case when the superposed free convection is weak [7]. Reduction of pressure loss due to the superposition of free convection is still found. More remarkable reduction of the total pressure loss is expected if the value of Gr/Re^2 can be brought higher.

Next, the effect of the offset length L of the flat plate will be discussed. In this case, the total depth of the system was unchanged so that the total number of the rows of plates is proportional to the reciprocal of L. Figures 15 and 16 show respectively the variation of $\overline{Nu}$ and $\overline{C_p^*}$ with the change of L. The obtained value of $\overline{C_p^*}$ is positive for all the computed conditions. This is because the flow is in the mixed convection flow regime. $\overline{Nu}$ increases as L is decreased. Thus, a shorter offset length of the plate is better for heat transfer performance. However, the increase of $\overline{Nu}$ with the decrease of L is rather small when $H/L > 5$. The same is also found for $\overline{C_p^*}$. Thus, excessive interruption of the heat transfer surface is not efficient and subsequently does not match its higher production cost. Incidentally, Figs. 15 and 16 show that $\overline{Nu}$ and $\overline{C_p^*}$ increase with an increase of Gr/Re^2 for any offset length of the flat plate. This is the effects caused by the superposed free convection.

Computations have also been made for the cases keeping the offset length of the flat plate constant but changing the total depth of the system. In these computations, the total depth is proportional to the total number of the rows of the flat plates. The computed results of $\overline{Nu}$ and $\overline{C_p^*}$ are plotted in Figs. 17 and 18. In the smallest case of Gr/Re^2, when the superposed free convection is weakest as seen from the value of $\overline{C_p^*}$ in Fig. 18, the value of $\overline{Nu}$ decreases as the total number of the rows N is increased. The velocity and thermal boundary layers become thicker on a flat plate at the location of larger depth, because the velocity defect and temperature defect do not recover completely in the wake region of each flat plate. This tends to deteriorate the heat transfer from one plate to another at larger depth in the system. Thus, the decrease of $\overline{Nu}$ with the increase of N is not surprising. However, even at this smallest value of Gr/Re^2, such a tendency

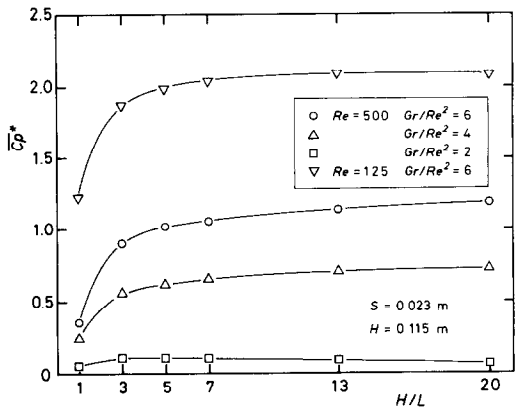

FIG. 16. Change of $\overline{C_p^*}$ with the offset length L.

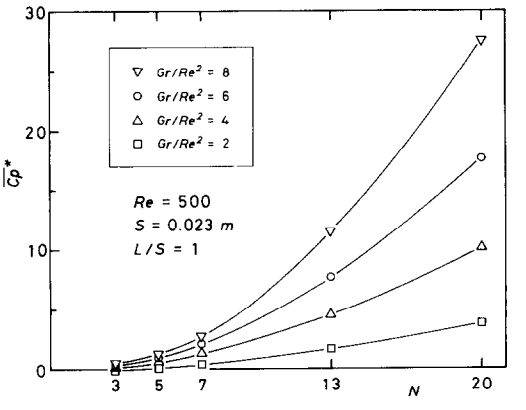

FIG. 18. Change of $\overline{C_p^*}$ with the total depth H.

becomes almost unremarkable when $N \geqslant 13$. This indicates that the velocity and thermal fields become fully developed at the depth after the first 13 rows. In the cases of larger value of Gr/Re^2, the decrease of $\overline{Nu}$ with the increase of N is less noticeable and $\overline{Nu}$ is found even increasing with the increase of N. From the results plotted in Fig. 17, better heat transfer performance may be expected to result from adding more module to the downstream end of heat exchanger, at least, when $Gr/Re^2 \geqslant 6$. This feature may be caused by the combination of the following three effects of the superposed free convection. (1) The flow acceleration continues to proceed in the wake of a flat plate because of the existing temperature defect in the wake. This is facilitated by the larger rate of the fluid entrainment into the wake. This means that the restoration from the temperature defect should also be accelerated. This faster restoration of the velocity and temperature defects leads to a condition of thinner velocity and temperature boundary layers to be formed around the next flat plate. This brings a tendency of less deterioration towards the downstream end of the system. (2) The augmentation of heat transfer due to the superposed free convection comes into effect only when the velocity profile is sufficiently distorted. As found in another simple flow situation [14], heat transfer enhancement occurs only after some distance from the inlet although the flow acceleration itself should start from the inlet. This suggests that, with larger depth of the heat transfer system, enhancement effects of superposed free convection is expected in a larger fraction of the total depth. (3) For the heat transfer system with uniform flat plate temperature, the bulk mean temperature of the fluid comes closer to the flat plate temperature toward the downstream end. This means that an excess gravitational force, which is effective in deforming the velocity profile, decreases toward the downstream end. However, as will presently be seen, this decreasing tendency is mitigated in the computed cases of downward flow cooled by the flat plates. This is because the variation of fluid properties occurs in such a way that the decrease of the effective local Grashof number toward the downstream end is suppressed [14].

In Figs. 15–18, the pitch between neighbouring flat plates, $2S$, was assumed to be constant value of 0.023 m. Therefore, it may be worthwhile to show additionally how this pitch affects the flow and heat transfer performance of the system. Two examples of this are shown in Figs. 19 and 20. In these calculations, the offset length of the plate L was not changed and the total number of the flat plate rows was also kept the same. The flat plate temperature was kept constant so that the value of Gr varies with the change in the value of S. The value of Gr/Re^2 was set in a way that its value at $S/L = 1$ is equal to 4. While the Reynolds number was kept constant in Fig. 19, the fluid inlet velocity was kept constant in Fig. 20. Therefore, in the former figure, the value of Gr/Re^2 varies proportional to S^3 but, in the latter figure, Gr/Re^2 varies proportionally with S. In the

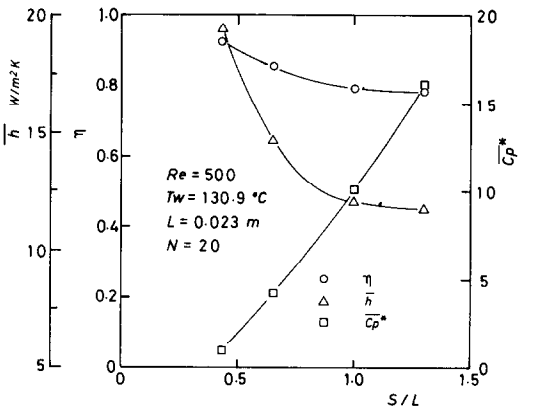

FIG. 19. Effects of fin pitch at constant Reynolds number.

latter case, the value of Re varies proportionally with S. In Fig. 20, the fluid inlet velocity was set in such a way that the value of Re at $S/L = 1$ is 500. Since the inclusion of $2S$ in the definition of $\overline{Nu}$ is inconvenient to see the effects of the plate pitch on the heat transfer performance, the mean heat transfer coefficient $\bar{h} = \lambda_0 \overline{Nu}/4S$ is plotted in Figs. 19 and 20. In these two figures, the recovery factor of available thermal energy η defined below is also plotted.

$$\eta = \frac{T_0 - T^*}{T_0 - T_w} \tag{11}$$

where T^* is the bulk mean temperature of the fluid at the outlet from the heat transfer system. The temperature difference $(T_0 - T_w)$ represents the amount of available thermal energy of waste gas at the inlet to the system and $(T_0 - T^*)$ represents the amount of recovered thermal energy. η may be expressed as

$$\eta = \xi \overline{St} \tag{12}$$

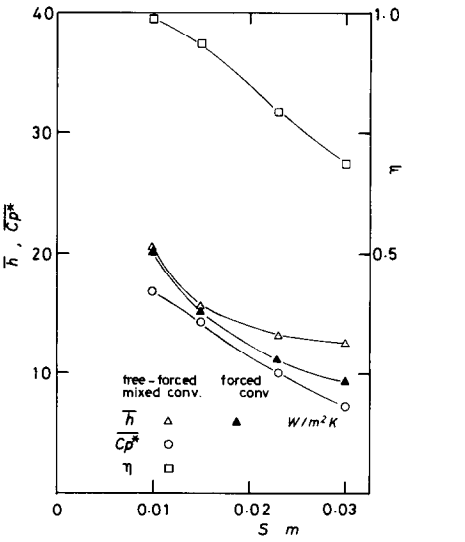

FIG. 20. Effects of fin pitch at constant gas velocity.

where ξ is the ratio between the total heat transfer surface area and the total frontal area of the system, NL/S, and represents the packing density of the heat transfer surface. The average Stanton number $\overline{St}$ has been defined as follows:

$$\overline{St} = \frac{1}{\rho_0 C_{p_0} U_0 (T_0 - T_w)} \frac{1}{H} \sum_{i=1}^{N} \int_{(i-1)L}^{iL} |q_w| \, dx. \quad (13)$$

Considering a case for which the increment of bulk mean temperature within the length L of a plate is much smaller than the temperature difference $(T_m - T_w)$ and the distribution of local Nusselt number Nu is approximately the same for all flat plates, the above relationship for $\overline{St}$ may be approximated by the following form:

$$\overline{St} = \frac{\overline{Nu}}{Re\ Pr} \frac{(\bar{T}_m - T_w)}{(T_0 - T_w)} \quad (14)$$

where $\bar{T}_m$ is the arithmetic mean of the bulk mean temperature of the fluid evaluated at the leading edge of the flat plate in every row. The following relationship is introduced here for $\overline{Nu}$.

$$\overline{Nu} = 0.664\ Pr^{1/3}\ Re^{1/2} \sqrt{4S/L}. \quad (15)$$

While the present flow is neither one of boundary-layer type nor one in pure forced convection regime as assumed in reducing equation (15), the above equation may be taken as a rule of thumb for the discussions of some features of the effects of geometrical parameters and fluid velocity.

In Fig. 19, the value of η is found to decrease rather moderately with an increase of S. This is because the decrease of the ratio ξ with the increase of S is compensated by the increase of $\overline{St}$. From equations (14) and (15), the value of $\overline{Nu}$, and therefore the value of $\overline{St}$, are expected to increase with the increase of S. Additionally, remarkable change in Gr/Re^2 results in an intensification of the superposed free convection with an increase of S leading to the magnification of the change of $\overline{St}$ with the change in S. Although the value of ξ decreases proportionally with reciprocal of S, the value of $\overline{C_p^*}$ increases steeply with the increase of S. This results also from the remarkable increase of Gr/Re^2. $\bar{h}$ is found to decrease in Fig. 19 when S is increased. This is reasonable from equation (15). Slightness of the decrease of $\bar{h}$ observed when S is increased from the value of $S/L = 1$ is again brought about by the large increase of Gr/Re^2.

In Fig. 20, $\overline{C_p^*}$ is found to decrease with an increase of S in an opposite way to the tendency found in Fig. 19. This is because the increase of Gr/Re^2 proportional to S is not effective enough to compensate for the reduction of the ratio ξ. The same reason leads to larger change in the recovery factor of available energy η. Another reason for this larger change of η is that the Reynolds number varies in Fig. 20 with the change in S. Because of this, in the light of equations (14) and (15), no direct increase of $\overline{St}$ is expected with an increase of S, contrary to the increasing tendency of $\overline{St}$ previously pointed out for Fig. 19.

The mean heat transfer coefficient $\bar{h}$ is found to decrease with the increase of S also in Fig. 20. This cannot be accounted for only by equation (15). To explain this point, several velocity distributions obtained at different streamwise locations for a pure forced convection regime are plotted in Fig. 21. It is found that the velocity defect in the wake of each plate is restored faster for smaller spacing between the neighbouring plates. This results in a larger gas approaching velocity for the flat plate in the next row and provides a condition for thinning the velocity and temperature boundary layers on that plate. This increases the heat transfer coefficient on that plate, and therefore, the value of $\bar{h}$ also. This is confirmed from the change of $\bar{h}$ for the pure forced convection regime which is also plotted in Fig. 20. The superposed free convection makes the problem a little more complicated in the free–forced mixed convection regime but not so much as altering the basic feature of the problem. The degree of the effects of superposed free convection may be guessed from the magnitude of deviation between the value of $\bar{h}$ for the free–forced mixed convection regime and its counterpart for pure forced convection regime. Faster restoration of the velocity defect in the wake for the case of smaller S found in Fig. 21 may have been caused by the fact that the deflection of streamlines due to the increase of displacement thickness on each plate is likely to extend to the wake region if the distance between the centre line of the wake and the neighbouring plate is smaller.

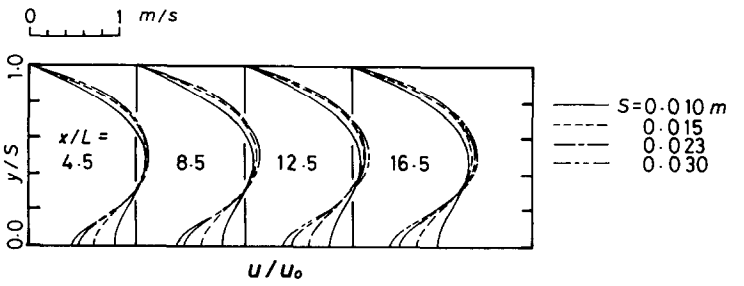

FIG. 21. Velocity distributions obtained for different fin pitch (pure forced convection flow regime).

For the heat exchanger to be used for extracting thermal energy from waste gas, to keep the value of η high is important. Moderate reduction in the value of η resulting from widening the fin space may be restored by lengthening the depth of the heat exchanger, if space is available for that. This may produce another desirable feature at the same time when the heat exchanger is used in the free–forced mixed convection regime. From the results in Fig. 18, higher values of pressure gain are then expected. Figure 17 indicates that even the value of $\overline{Nu}$ can also be increased then if the value of Gr/Re^2 is as high as 6.

5. CONCLUDING REMARKS

Experimental and numerical research has been done for a two-dimensional model of the offset-strip-fin type compact heat exchanger to be used at low Reynolds number in the free–forced mixed convection regime.

The two numerical schemes used in the present study have been confirmed to give almost the same results for the heat transfer characteristics of the two-dimensional model. Numerical computations taking account of the finite thickness of the plates and of the free-stream turbulence have been validated through comparing the computed results with the present experimental results. The present two-dimensional computation is in qualitatively good agreement with the performance study for the practical offset-strip-fin type heat exchanger in the range of Reynolds number of $Re <$ 800. It is found that there is no good reason to prefer thicker fins for the heat exchanger to be used for the purpose of thermal energy recovery from waste gas. Shorter fin offset length gives better heat transfer performance but interruption of fins too often is not efficient enough to justify its higher production cost. Larger depth of the heat exchanger leads to better performance, especially, when the available level of Gr/Re^2 is as high as 6. For the heat exchanger to be used for the purpose presently concerned, the dense packing may not be the crucial requirement. Moderate deterioration of the performance caused by the larger fin pitch may be restored by lengthening the depth of the heat exchanger when space is available for that.

REFERENCES

1. A. L. London and R. K. Shah, Offset rectangular plate–fin surface—heat transfer and flow friction characteristics, *J. Engng Pwr* **89,** 218–228 (1968).
2. S. Mochizuki and Y. Yagi, Heat transfer and friction characteristics of strip fins, *Heat Transfer—Jap. Res.* **6,** 36–59 (1977).
3. E. M. Sparrow, B. R. Boliga and S. V. Patankar, Heat transfer and fluid flow analysis of interrupted wall channels with application to heat exchanger, *J. Heat Transfer* **99,** 4–11 (1977).
4. E. M. Sparrow and C. Prakash, Enhancement of natural convection heat transfer by a staggered array of discrete vertical plates, *J. Heat Transfer* **102,** 215–220 (1980).
5. N. Cur and E. M. Sparrow, Experiments on heat transfer and pressure drop for a pair of colinear interrupted plates aligned with the flow, *Int. J. Heat Mass Transfer* **21,** 1069–1080 (1978).
6. S. V. Patankar and C. Prakash, An analysis of the effect of plate thickness on laminar flow and heat transfer in interrupted plate passage, *Int. J. Heat Mass Transfer* **24,** 1801–1810 (1981).
7. K. Suzuki, E. Hirai, T. Sato and S. Kieda, Numerical study of heat transfer system with staggered array of vertical flat plates used at low Reynolds number, *Proc. 7th Int. Heat Transfer Conf.*, vol. 3, pp. 483–488 (1982).
8. Y. Kang and K. Suzuki, Numerical study of wall heat transfer in the recirculating flow region of a confined jet, *Heat Transfer—Jap. Res.* **11,** 44–69 (1982).
9. K. Suzuki, T. Sato, Y. Kang and T. Sugimoto, Circular tube turbulent heat transfer in the downstream of an orifice, *Heat Transfer—Jap. Res.* **11,** 70–90 (1982).
10. A. D. Gosman, W. M. Pun, A. K. Runchal, D. B. Spalding and M. Wolfstern, *Heat and Mass Transfer in Recirculating Flows.* Academic Press, London (1969).
11. W. M. Pun and D. B. Spalding, A general computer program for two dimensional elliptic flows, Imperial College Mechanical Engineering Department Report HTS/76/2 (1976).
12. S. Kieda and K. Suzuki, Numerical study of the flow passing a flat plate of finite length, *Trans. Japan Soc. mech. Engrs* **46,** 1655–1661 (1980).
13. S. Kieda, K. Suzuki and T. Sato, Numerical study on flow behaviour and heat transfer in the vicinity of starting point of transpiration, numerical methods, in *Laminar and Turbulent Flow* (edited by C. Taylor and B. A. Schrefler). Pinneridge Press, Swansea (1981).
14. K. Suzuki, S. Kieda, T. Chichiki and T. Sato, Numerical study of combined convective heat transfer with variable fluid properties in the inlet region of a circular tube, in *Numerical Methods in Thermal Problems* (edited by R. W. Lewis *et al.*). Pinneridge Press, Swansea (1981).
15. P. J. Roache, *Computational Fluid Dynamics.* Hermosa, Albuquerque, New Mexico (1972).
16. S. V. Patankar, A numerical method for conduction in composite materials, flow in irregular geometries and conjugate heat transfer, *Proc. 6th Int. Heat Transfer Conf.*, vol. 3, pp. 297–302 (1978).
17. B. E. Launder and D. B. Spalding, The numerical computation of turbulent flows, *Comput. Meth. appl. Mech. Engng* **3,** 269–289 (1974).
18. W. P. Jones and B. E. Launder, The prediction of laminarization with a two-equation model of turbulence, *Int. J. Heat Mass Transfer* **15,** 301–314 (1972).
19. O. A. Plumb and L. A. Kennedy, Application of a k–ε turbulence model to natural convection from a vertical isothermal surface. *J. Heat Transfer* **99,** 79–85 (1977).
20. A. A. Townsend, Equilibrium layers and wall turbulence, *J. Fluid Mech.* **11,** 97–120 (1961).
21. W. J. Yang, Forced convective heat transfer in interrupted compact surfaces, *ASME–JSME Thermal Engineering Joint Conference Proceedings*, vol. 3, pp. 105–111 (1983).
22. S. Mochizuki and Y. Yagi, Characteristics of vortex shedding in plane arrays, flow visualization II (edited by W. Merzkirch), pp. 99–103. Hemisphere, Washington D.C. (1982).
23. D. D. Gray and A. Giorgini, The validity of the Boussinesq approximation for liquids and gases, *Int. J. Heat Mass Transfer* **19,** 545–551 (1976).

ETUDE NUMERIQUE ET EXPERIMENTALE SUR UN MODELE BIDIMENSIONNEL D'AILETTE EN RUBAN D'UN ECHANGEUR COMPACT UTILISE AUX FAIBLES NOMBRES DE REYNOLDS

Résumé—On présente une étude numérique et expérimentale de l'écoulement et des caractéristiques thermiques pour un système bidimensionnel avec un arrangement étagé de plaques planes verticales utilisé pour le régime de convection mixte aux faibles nombres de Reynolds. Les schémas numériques utilisés sont validés à travers la comparaison des résultats numériques et des données expérimentales obtenus dans cette étude. On discute les effets de l'épaisseur de l'ailette et de la turbulence de l'écoulement. Des comparaisons sont aussi faites entre le présent calcul en bidimensionnel et les données expérimentales pour un échangeur compact à ailettes eu ruban et on ajoute des commentaires sur les effets de la tridimensionnalité. On présente enfin la discussion des effets de quelques paramètres géométriques de l'échangeur sur ces performances, à partir des présents travaux numériques.

ZWEIDIMENSIONALE NUMERISCHE UND EXPERIMENTELLE UNTERSUCHUNG EINES 'OFFSET-STRIP-FIN'-KOMPAKTWÄRMETAUSCHERS BEI KLEINEN REYNOLDS-ZAHLEN

Zusammenfassung—Bei der Mischkonvektion in einer zweidimensionalen gestaffelten Anordnung von senkrechten ebenen Platten wurden Strömung und Wärmeübergang bei kleinen Reynolds-Zahlen numerisch und experimentell untersucht. Dabei wurde das numerische Modell anhand der Meßdaten bestätigt. Bei diesem Vergleich werden die Einflüsse von Rippendicke und Freistrahlturbulenz diskutiert. Die Ergebnisse des zweidimensionalen Rechenmodells werden darüber hinaus mit Versuchsergebnissen von praktisch ausgeführten 'offset-strip-fin'-Wärmetauschern verglichen. Der Einfluß dreidimensionaler Vorgänge wird erörtert. Anhand der numerischen Ergebnisse wird der Einfluß der Geometrie auf die Leistung des Wärmetauschers dargestellt.

ЧИСЛЕННОЕ И ЭКСПЕРИМЕНТАЛЬНОЕ ИССЛЕДОВАНИЕ ДВУМЕРНОЙ МОДЕЛИ КОМПАКТНОГО ТЕПЛООБМЕННИКА С ПЛАСТИНЧАТЫМИ РЕБРАМИ ПРИ МАЛЫХ ЧИСЛАХ РЕЙНОЛЬДСА

Аннотация—Проведены численные и экспериментальные исследования характеристик течения и теплообмена двумерной системы с шахматным расположением вертикальных плоских пластин в диапазоне малых чисел Рейнольдса в режиме смешанной конвекции. Применяемые числовые схемы обосновываются путем сравнения численных результатов с соответствующими экспериментальными данными, полученными в работе. Анализируется влияние толщины ребра и турбулентности свободного потока. Проведено сравнение между представленными расчетами для двумерного случая и экспериментальными данными для реального компактного теплообменника с пластинчатыми ребрами, отмечается влияние трехмерности. В заключение рассмотрено основанное на численных расчетах влияние геометрических параметров теплообменника на его эффективность.